ELSEVIER

Journal of Power Sources 62 (1996) 149–154

JOURNAL OF POWER SOURCES

Synthesis and characterization of lithium intercalation electrodes based on iron oxide thin films

J. Sarradin, A. Guessous, M. Ribes

Laboratoire de Physicochimie de la Matière Condensée, UMR 5617, Université Montpellier II, place Eugène Bataillon, 34095 Montpellier Cedex 5, France

Received 19 October 1995; revised 12 April 1996; accepted 29 April 1996

Abstract

Sputter-deposited iron oxide thin films are investigated as a possible negative electrode for rocking-chair microbatteries. Experimental conditions related to the manufacturing of amorphous thin films suitable to a large number of available intercalation sites are described. Structural and physical properties of the thin layer films are presented. The conductivities of the amorphous thin films were found to be very high compared with those of the respective crystalline forms. Regarding the electrochemical behaviour, Fe_2O_3-based thin films electrodes are able to store and reversibly exchange lithium ions. At a $C/2$ charge/discharge rate with 100% depth-of-discharge (DOD), the specific capacity of these amorphous thin film electrodes remains almost constant and close to 330 Ah/kg after more than 120 charge/discharge cycles.

Keywords: Iron oxide; Thin films; Electrodes; Lithium

1. Introduction

Research concerning the development of miniaturized systems for energy storage, such as microbatteries, has known a growing interest during the last decade. The fabrication of microbatteries results from stacking of several thin films. In general, glasses and amorphous materials are well suited to the production of thin films by techniques such as reactive r.f. sputtering or vacuum evaporation.

Mixed conductive glasses and/or amorphous materials can be used as the anode or cathode materials. So far, all microbatteries studied or developed on laboratory scale include a lithium metal anode [1–4].

The use of lithium metal as the negative electrode in rechargeable batteries introduces some problems, e.g. the cycleability of these cells. Also, the replacement of the lithium metal — using the rocking-chair [5] or lithium-ion concept — by an anodic material able to store and exchange one or more lithium ions would help the present limitations of rechargeable batteries, which are mainly due to the large reactivity of this metal, to be solved.

Another problem linked to the rechargeable batteries concerns the characteristics of cathodic or anodic materials. An electrochemical cycle is often accompanied by a change in lattice dimension of the host structure and capacity losses observed in these cells may be the result of the partial destruction of the core structure.

Amorphous insertion materials whose change in lattice dimension is strongly reduced [6,7] or zero strain insertion materials [8] whose lattice dimension does not change seem to be ideal materials electrodes for rocking-chair batteries.

However, the feasibility of a rocking-chair battery requires to meet some crucial conditions [9]:

(i) the lithium activity in the negative electrode has to be close to 1, assuming a high open-circuit voltage (OCV) of the battery;

(ii) the variations of potential of both electrodes need to be small during the charge/discharge cycles, and

(iii) the specific capacity of the negative electrode should be as high as possible compared with the very low equivalent weight of the lithium metal.

Although (iii) is not of great importance in the case of microbatteries, few materials will meet the above-mentioned properties and are able to replace the lithium electrode. Carbon in various forms is well known and already used in commercial cells [10]. Some oxides such as WO_2, Fe_2O_3 [11,12] and low voltage spinels [13] are also possible candidates to be used as the negative electrode in rocking-chair batteries.

This paper reports on iron oxides and especially on amorphous Fe_2O_3 thin films, because they exhibit the two following major advantages:

(i) the high theoritical specific capacity of this material ($Li_6Fe_2O_3 \approx 1000$ Ah/kg); this capacity is available in a voltage range below 1 V versus Li, and

PII S0378-7753(96)02429-9

(ii) the possibility to obtain an amorphous state of this material by means of deposition techniques such as r.f. sputtering.

The amorphous state presents an interesting characteristic regarding the intercalation/de-intercalation process. The 'open' structure gives rise to a large number of available intercalation sites [14] and, therefore, the volume variation of the electrode is limited during the intercalation/de-intercalation process.

This fact is well known for a cathodic material such as V_2O_5 since during the intercalation process of lithium ions in an amorphous or vitreous V_2O_5, the change in volume corresponds to 5% compared with 16% observed on the same crystalline material [7].

If there is no destruction of the 'structure' in an amorphous material, the electrochemical characteristics of the electrode are better, and thus improving the cycleability of our electrode, one of the major characteristics needed in the rocking-chair concept.

2. Experimental

Amorphous iron oxide thin films were obtained by r.f. sputtering from α-Fe_2O_3 and/or Fe_3O_4 targets (2′ϕ, Cerac 99.9 and 99%, respectively). Argon plasma is used to fabricate thin films from the α-Fe_2O_3 target while nitrogen plasma is needed to deposit the thin films from the Fe_3O_4 target. The rate deposition depends on the nature of the plasma ($\approx$560 and $\approx$280 Å/h under argon and nitrogen, respectively). The thin films were investigated by means of X-ray analyses (Seifert MZ 4) in order to check either the amorphous or the crystalline nature of the layers.

The scanning electron microscope analyses (SEM) (CAMBRIDGE 360) allows the morphology of the thin films to be observed and their thickness to be measured.

^{57}Fe conversion electron Mössbauer spectroscopy (CEMS) was used to study the local environment of iron into the thin films.

Alumina substrates with platinum contacts elaborated by the thick film fabrication technique were used as conductivity cells.

The conductivity measurements were performed in an evacuated Pyrex chamber connected to an impedance analyser (Hewlett-Packard 4192 A) driven by a computer.

All electrochemical measurements were carried out in an argon filled dry box. Propylene carbonate (PC) from Burdick and Jackson was dried over 4 Å molecular sieves (Aldrich) prior to use. 1 M solution of lithium hexafluoroarsenate (Aldrich) in PC was used as the electrolyte solution for the test cells.

The lithium cells consist of two lithium wires (counter and reference electrodes) and a thin film of the iron oxide deposited on a thin layer of chromium previously sputter-deposited onto a glassy substrate. The electrodes were prepared electrochemically by passing a known quantity of electricity in the cell.

The cycling tests were carried out automatically by means of a scanning potentiostat (EGG/PAR 362). The OCVs were measured using a very high impedance voltmeter (Radiometer Analytical S.A./Tacussel Minisis 8000).

3. Results and discussion

3.1. Chemical and physical characteristics of the iron oxide thin films

The following iron oxide thin films were studied:

(i) thin films corresponding to the layers manufactured from the α-Fe_2O_3 target under an argon plasma, and

(ii) thin films corresponding to the layers manufactured from the Fe_3O_4 target under a nitrogen plasma. Some of these layers were thermally annealed in order to obtain a so-called 'γ-Fe_2O_3'.

3.1.1. SEM study

Figs. 1 and 2 show the cross-sectional view and the surface aspects of iron oxide thin films. A sputter-deposited thin film from the α-Fe_2O_3 target elaborated under argon can be

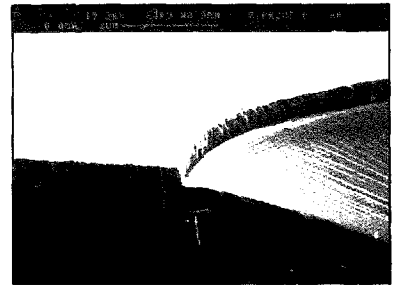

Fig. 1. SEM cross-sectional view of a sputter-deposited thin film fabricated from the α-Fe_2O_3 target under argon plasma.

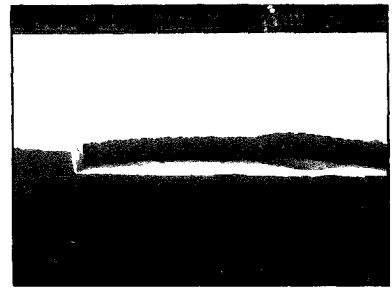

Fig. 2. SEM cross-sectional view of a sputter-deposited thin film fabricated from the Fe_3O_4 target under nitrogen plasma.

observed in Fig. 1. For this sample deposited onto a glass substrate, its thickness is close to 3500 Å. The deposition time was 6 h.

Fig. 2 shows a sputter-deposited thin film from the Fe_3O_4 target fabricated under nitrogen plasma. Its thickness is also close to 3500 Å. However, in this case, the deposition time was 12 h.

In both cases, a columnar structure characteristic of the r.f. sputtering process is observed. Regarding the rate deposition, the growth of the layer depends on the plasma used. Under argon plasma, the rate deposition is twice as great as the rate obtained under nitrogen plasma, but a nitrogen plasma is needed during the deposits carried out from the Fe_3O_4 target in order to avoid a modification/oxidation of the target as well as the deposit of thin films whose composition should be closer to Fe_2O_3 than to Fe_3O_4.

3.1.2. X-ray study

In our experimental conditions, whether we used the argon or the nitrogen plasma r.f. techniques to elaborate the thin films, all the layers manufactured were amorphous.

The problem concerning the amorphous deposits is related to the knowledge of the real nature of our thin layers. Unsuccessfully, we tried to crystallize iron oxide thin films previously deposited on silica substrates. Samples obtained from the α-Fe_2O_3 and Fe_3O_4 targets were fired at 600 °C in open air and under nitrogen, respectively. No crystallization peak appeared during X-ray analyses and all the deposits remained amorphous. The size of crystallites may be a decisive factor. Investigations regarding this point are currently in progress.

3.1.3. Conversion electron Mössbauer spectroscopy study

$Li_xFe_2O_3$ samples were already studied by Mössbauer spectroscopy but only bulk samples [15].

^{57}Fe conversion electron Mössbauer spectroscopy (CEMS) can be usefully applied to study the local environment of iron in thin films because it investigates only the surface layer of solids (2000 Å thick) at a thickness comparable with that of our films. Two iron oxide thin film samples were investigated by CEMS at room temperature:

(i) sample #1 obtained from the α-Fe_2O_3 target under argon plasma, and

(ii) sample #2 obtained from the Fe_3O_4 target under nitrogen plasma.

Sample #1 exhibits a magnetically split pattern as the main component of the spectrum (≈ 87%) and a broadened single line (≈ 13%) as shown in Fig. 3.

The hyperfine interaction parameters of the main component (isomer shift, S, quadrupole splitting, QS, and hyperfine magnetic field, H) are very close to those in Fe_2O_3 [16]. Non-Lorentzian line shape of the main component implies that a distribution of the hyperfine interaction parameters, in particular of the hyperfine magnetic field, H, should be taken into account in analysing the spectrum. A modified method of discrete step functions by Hesse and Rübartsch [17] was

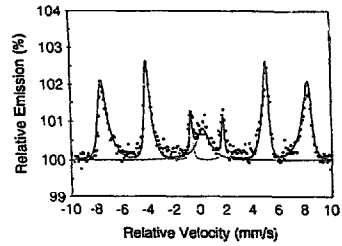

Fig. 3. Typical ^{57}Fe conversion electron Mössbauer spectroscopy of a sputter-deposited thin film fabricated from the α-Fe_2O_3 target under argon plasma.

used to obtain a distribution function of the hyperfine magnetic field, P(H). The derived P(H) is shown in Fig. 4.

The distribution is peaked at ≈ 486 kOe which is less than H = 515–518 kOe characteristic of bulk α-Fe_2O_3 particles [18] and Fe^{III} oxide aggregates in a glassy matrix [19] of a mean size more than ≈ 14 nm. Therefore, broad non-Lorentzian lines and the reduced value of the effective hyperfine magnetic field imply that the Fe^{III} oxide species in the sample #1 are amorphous or microcrystalline. The asymmetric distribution function P(H) shown in Fig. 4 may also indicate that some distribution in the average dimensions of different amorphous and/or microcrystalline Fe_2O_3 particles exists in the sample (uniform amorphous network is characterized by nearly Gaussian distribution) or, alternatively, the low-field side of the distribution corresponds to Fe^{III} oxide species originating from another modification of Fe^{III} oxide (for example, γ-Fe_2O_3). The second component, a broadened line with S = 0.17 mm/s relative to α-Fe, corresponds to paramagnetic Fe^{III} ions in a tetrahedral environment.

Sample #2 exibits also a magnetically split spectrum as shown in Fig. 5.

In contrast to sample #1 with different well-defined Fe^{III} oxide species, multiple iron oxide sites in sample #2 are not very well distinguished from each other. As a result, rather poorly resolved resonance pattern are observed. However, an

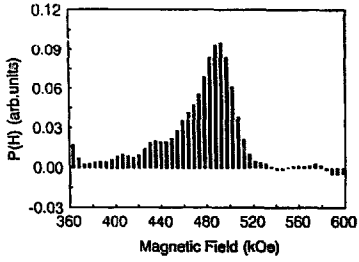

Fig. 4. Distribution fonction of the hyperfine magnetic field for a magnetically split component in the spectrum of a sputter-deposited thin film fabricated from the α-Fe_2O_3 target under argon plasma.

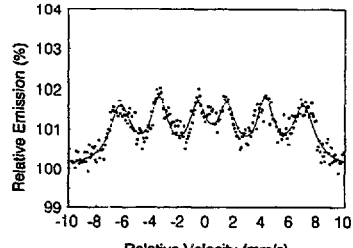

Fig. 5. Typical ^{57}Fe conversion electron Mössbauer spectroscopy of a sputter-deposited thin film fabricated from the Fe_3O_4 target under nitrogen plasma.

essential feature can be extracted from the spectrum. The average effective hyperfine magnetic field in sample #2 ($\simeq$410 kOe) is much less than that in sample #1. It means that the local environment of iron is, probably, closer to that in Fe_3O_4, where the values of H for two different sublattices are $\simeq$450 and $\simeq$480 kOe, respectively. The ratio Fe^{III}:Fe^{II} is 2 in this oxide. However, it seems to be difficult to determine the minor Fe^{II} oxide fraction in the spectrum of sample #2, which can be lower than 0.33, because of its complexity.

3.1.4. Conductivity study

Impedance spectroscopy (5 Hz–13 MHz) was used to measure the electrical characteristics of the samples. In order to obtain an Arrhenius plot of electrical conductivity, iron oxide thin films were heated between room temperature and 180 °C under vacuum. Fig. 6 gives the values obtained from three iron oxide thin films:

(i) sample A fabricated from the α-Fe_2O_3 target under argon plasma;

(ii) sample B fabricated from the Fe_3O_4 target under nitrogen plasma, and

(iii) sample C from the Fe_3O_4 target previously elaborated under nitrogen plasma and annealed during 2 h at 350 °C in

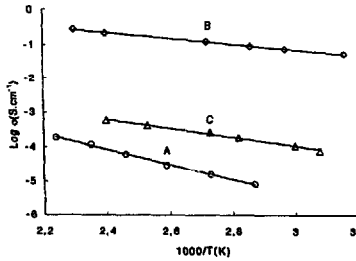

Fig. 6. Arrhenius plot of electrical conductivity of a sputter-deposited sample fabricated under argon plasma from the (A) α-Fe_2O_3 target, (B) of a sputter-deposited sample elaborated under nitrogen plasma from the Fe_3O_4 target, and (C) an annealed sample previously fabricated from the Fe_3O_4 target under nitrogen plasma.

Table 1
Electrical characteristics of iron oxide thin films

Samples	A	B	C
Activation energy (eV)	0.45	0.16	0.26
Conductivity at room temperature (S cm^{-1})	6.5×10^{-7}	3.7×10^{-2}	3.8×10^{-5}

open air; this thermal treatment is carried out in order to achieve the well-known transformation occurring when the crystalline form is heated

$$1/2O_2 + 2Fe_3O_4 \rightarrow 3\gamma\text{-}Fe_2O_3 \quad (1)$$

Table 1 summarizes the electrical characteristics of these samples. Sample A exhibits a conductivity close to 5×10^{-7} S cm^{-1}. This value is very high compared with the value of the bulk material since the conductivity of the crystalline α-Fe_2O_3 powder is about 1×10^{-13} S cm^{-1} [11].

Regarding sample B, its conductivity value is close to 5×10^{-2} S cm^{-1}. This value is higher than that measured on the crystalline Fe_3O_4 powder (5×10^{-4} S cm^{-1}). After the annealing treatment, sample C remains amorphous. However, as a consequence, the thermal treatment seems to achieve the transformation '$Fe_3O_4 \rightarrow Fe_2O_3$' as the conductivity measured on this sample is very close to that of a crystalline γ-Fe_2O_3 powder, i.e. 1×10^{-5} S cm^{-1} [11].

Summarizing the results regarding the chemical and physical characteristics of our iron oxide thin films obtained via r.f. sputtering, two main conclusions may be drawn:

(i) All the samples elaborated from the α-Fe_2O_3 target under argon plasma are amorphous and contain only the Fe^{III} specie. The measured value of conductivity (5×10^{-7} S cm^{-1}) can be regarded as the result of a mixture of 'γ-Fe_2O_3/α-Fe_2O_3' whose conductivities in their crystalline forms are ranging from 1×10^{-5} S cm^{-1} to 1×10^{-13} S cm^{-1}, respectively.

(ii) All the samples from the Fe_3O_4 target elaborated under nitrogen plasma are amorphous and contain a mixture of the Fe^{III} and Fe^{II} species. After the thermal treatment mentioned above, a conductivity very close to that of the crystalline 'γ-Fe_2O_3' form is obtained.

3.2. Electrochemical behaviour

Associated with the advantageous amorphous nature of our deposits there are net benefits to use thin films as the electrodes of batteries:

(i) the small thickness of the active material allows an easier diffusion of the lithium ions throughout the layer;

(ii) a large number of electrodes can be stacked for example in a unit cell, and

(iii) the thin film technique allows to use cathodic or anodic materials whose conductivities are in the 10^{-7}–10^{-8} S cm^{-1} range at room temperature. This point is of great importance in all solid-state microbatteries (total thickness

≈ 10 μm) including of course a thin layer of solid electrolyte (Li^+-ion conducting).

In such solid-state microbatteries, the current density is usually in the 10–50 μA/cm² range. The calculated value of the ohmic drop due to the internal resistance of 1 cm² electrode whose conductivity is, for example, 1×10^{-8} S cm^{-1} is acceptable if the thickness of the thin film does not exceed 1 μm. The same calculation is valid for a thickness close to 1 mm but gives rise to a huge ohmic drop excluding for that kind of material the utilization of thick electrodes.

So far, electrodes based on crystalline α-Fe_2O_3 contained a small quantity of carbon or graphite in order to improve the electronic conductivity of this material.

However, the addition of a binder and/or graphite decreases the specific capacity of these electrodes. Our electrodes are graphite-free ones and are used as-received after being r.f.-sputtered.

We focused especially our experiments on thin film electrodes fabricated from the α-Fe_2O_3 target under argon plasma, but, nevertheless, some annealed thin film electrodes, previously elaborated under nitrogen plasma from the Fe_3O_4 target, were also investigated. Prior to iron oxide thin films deposits, all the electrodes were coated with a chromium thin layer in order to obtain a strong adhesive collector. Cycling of the thin film electrodes was carried out galvanostatically at a current density of 100 μA/cm² between 3.2 and 0.3 V versus Li. Charge/discharge cycles were carried out close to a C/2 rate, based on the first charge/discharge cycle.

Regarding the determination of the electrode mass, our procedure was similar to the technique used by teams working in the field of microbatteries [20]. Knowing the thickness (by SEM) and the area, and using an assumed density 5.2 g/cm³, we were able to obtain the thin film mass.

3.2.1. *Annealed thin film electrodes*

Few experiments were carried out on that kind of electrodes owing to the difficulty to know the actual nature of the deposit (Fe_3O_4/Fe_2O_3) and as a consequence to obtain the correct number of Faraday per mole. 1 cm² area electrodes were reduced or charged in lithium at a current density of 100 μA/cm². Based on a supposed Fe_2O_3 deposit, result of the annealing treament, and knowing the thickness of the thin film, a specific capacity ≈ 280 Ah/kg was obtained as shown in Fig. 7 after about 30 charge/discharge cycles. This value corresponds to 1.7 Li/Fe_2O_3.

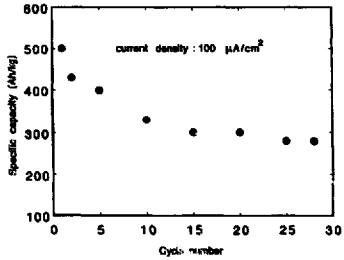

Fig. 7. Cycle number vs. specific capacity for an annealed thin film electrode previously fabricated from the Fe_3O_4 target under nitrogen plasma.

Experiments are currently in progress in order to study the behaviour of these thin film electrodes with long-term cycling conditions as well as the importance of the annealing treament on the electrochemical characteristics of the electrodes.

3.2.2. *Thin film electrodes elaborated under argon plasma from the α-Fe_2O_3 target*

Similar size electrodes (1 cm²) were used in these experiments. In that case, according to the Mössbauer results, only Fe^{III} species were present in the electrodes, i.e. the Fe_2O_3 form. In the Fig. 8, the charge process is corresponding to the uptake of lithium ions into the iron thin film electrode; their release is occurring during the discharge process.

Curves A show the results obtained during charge/discharge cycle #1. A plateau at 0.7 V versus Li was observed and around 5 Li were intercalated while only 4 Li were restituted. During charge/discharge cycle #70 (curves B), the amount of intercalated lithium is close to 2.4. Then, this quantity is slightly decreasing from cycle #70 to cycle #120. At this point (curves C), the amount of intercalated lithium is equal to 2.

If we consider the intercalated amount of lithium during the charge process, this quantity trends towards 2 Li/Fe_2O_3 corresponding to a specific capacity close to 330 Ah/kg. The decay in cycling capacity observed in Fig. 9 might be the result of a too high charge/discharge rate associated to 100% DOD. We are presently modifying the experimental conditions in order to analyse their influence on the cycle life.

It is interesting to point out that 2 Li/Fe_2O_3 is the disproportionation limit occurring on crystalline α-Fe_2O_3 during the electrochemical lithiation [21] although based on this structure, 4 Li/α-Fe_2O_3 are the maximum amount of lithium which can be inserted without a breakdown of the structure [11]. In our conditions, it appears that the amorphous nature of the deposit does not improve the amount of lithium to be

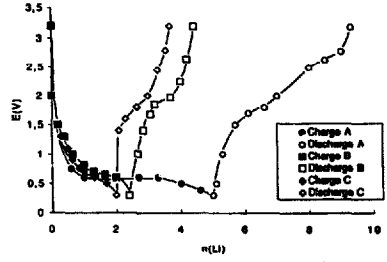

Fig. 8. Charge/discharge curves, lithium intercalation/de-intercalation cycles of the electrodes fabricated, under argon plasma, from the α-Fe_2O_3 target, $LiAsF_6$/PC electrolyte, and current rate = 100 μA/cm² (A) cycle #1; (B) cycle #70, and (C) cycle #120.

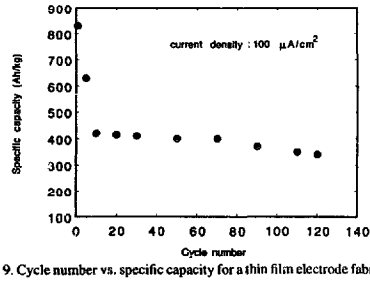

Fig. 9. Cycle number vs. specific capacity for a thin film electrode fabricated under argon plasma from the α-Fe_2O_3 target.

inserted. However, after 120 charge/discharge cycles, the remaining value of the specific capacity at about 330 Ah/kg (based on Fe_2O_3) seems an interesting characteristic which may be the result of the initial amorphous nature of the deposit [22].

4. Conclusions

Amorphous thin films based on iron oxides have been developed for insertion electrodes. These electrodes exhibit special characteristics due to their fabrication process. Sputtered layers, especially the amorphous thin films prepared under argon from the α-Fe_2O_3 target present a conductivity very high compared with that of crystalline α-Fe_2O_3 form. Such characteristics associated with the amorphous nature of the deposit give rise to a good electrochemical reversibility more than 120 charge/discharge cycles being performed on these electrodes. In spite of drastic running conditions, i.e. a C/2 cycle rate with 100% DOD, the specific capacity remains nearly constant and close to 330 Ah/kg. As a consequence, an interesting development of the cycleability of such electrodes may be expected. Experiments are currently in progress in order to optimize the cycling conditions, i.e. a limited DOD and lower cycling rates. All these experiments were carried out on small size electrodes but in the future, larger area electrodes will be investigated. The association of these electrodes with similar thin films cathodes already studied in our laboratory is planned in order to build up a rocking-chair battery.

Acknowledgements

The authors wish to thank Dr V. Semenov and Dr E. Bychkov for CEMS study and ANVAR for providing financial support (contract A 9311200 B).

References

[1] J.B. Bates, N.J. Dudney, G.R. Gruzalski, R.A. Zuhr, A. Choudhury and C.F. Luck, *J. Power Sources, 43/44* (1993) 103.
[2] S.D. Jones and J.R. Akridge, *J. Power Sources, 43/44* (1993) 505.
[3] G. Meunier, R. Dormoy and A. Levasseur, *Thin Solid Films, 205* (1991) 213.
[4] A. Guessous, J. Sarradin, A. Pradel and M. Ribes, *Solid State Ionics, 70/71* (1994) 368.
[5] M. Armand, in D.W. Murphy, J. Broodhead and B.C.H. Steele (eds.), *Materials for Advanced Batteries*, Plenum, New York, 1980, p. 145.
[6] S. Courant, M.J. Duclot, T. Pagnier and M. Ribes, *Solid State Ionics, 15* (1985) 147.
[7] M. Levy, F. Rousseau and M.J. Duclot, *Solid State Ionics, 28–30* (1988) 736.
[8] T. Ohzuku, A. Ueda and N. Yamamoto, *J. Electrochem. Soc., 142* (1995) 1431.
[9] B. Scrosati, *J. Electrochem. Soc., 139* (1992) 2776.
[10] T. Nagaura and K. Towaza, *Prog. Batteries Solar Cells, 9* (1990) 209.
[11] K.M. Abraham, D.M. Pasquariello and E.B. Willstaedt, *J. Electrochem. Soc., 137* (1990) 743.
[12] B. Di Pietro, M. Patriarca and B. Scrosati, *J. Power Sources, 8* (1982) 289.
[13] E. Ferg, R.J. Gummow, A. de Kock and M.M. Thackeray, *J. Electrochem. Soc., 141* (1994) L147.
[14] J.L. Souquet, A. Kone and M. Levy, in J.R. Akridge and M. Balkanski (eds.), *Solid State Microbatteries, Nato ASI Ser., 217* (1990) 301.
[15] S. Morzilli, B. Scrosati and F. Sgarlata, *Electrochim. Acta., 30* (1985) 1271.
[16] L.H. Bowen, *Datenjournal, 2* (1979) 76.
[17] J. Hesse and A. Rubartsch, *J. Phys., E7* (1974) 526.
[18] W. Kundig, H. Bommel, G. Constabaris and R.H. Lindquist, *Phys. Rev., 142* (1966) 327.
[19] E. Bychkov, M. Bruns, U. Geckle, W. Hoffmann, R. Schlesinger and H.J. Ache, *Solid State Ionics, 74* (1994) 165.
[20] J.B. Bates, D. Lubben, N.J. Dudney and F.X. Hart, *J. Electrochem. Soc., 142* (1995) L 149.
[21] M.M. Thackeray, W.I.F. David and J.B. Goodenough, *Mater. Res. Bull., 17* (1982) 785.
[22] A. Guessous, J. Sarradin and M. Ribes, *Fr. Patent No. 95 07 757* (1995).